Magnetic circular dichroism of the 1.404-eV interstitial nickel absorption transition in high-pressure synthetic diamond

P. W. Mason,* F. S. Ham, and G. D. Watkins
Department of Physics, Lehigh University, Bethlehem, Pennsylvania 18015
(Received 29 March 1999)

A high-resolution magnetic circular dichroism (MCDA) study of the sharp 1.404-eV zero-phonon absorption line associated with interstitial nickel in high-pressure synthetic diamond is reported. A model is presented attributing the absorption to internal transitions within the $3d^9$ configuration of Ni_i^+, as perturbed by the cubic field at the diamond interstitial site, plus a smaller trigonal crystal field. The model provides a consistent explanation of the signs of the circular absorption coefficients of all the observed transitions plus the unusual features of the g values observed for the ground ($g_\perp \sim 0$) and excited ($g_\parallel \sim 0$) states. A search for an optically detected magnetic resonance in the MCDA was unsuccessful, consistent with the forbidden magnetic resonance transition for an $S=1/2$, $g_\perp = 0$ ground state. [S0163-1829(99)13231-4]

I. INTRODUCTION

Ni is used as a catalyst in the high-temperature, high-pressure growth of synthetic diamond, and is therefore a likely contaminant. A recent electron paramagnetic resonance (EPR) study by Isoya *et al.*[1] has observed a defect (NIRIM-2) with an effective spin $S=1/2$ that possesses $\langle 111 \rangle$ trigonal symmetry with $g_\parallel = 2.3285$ and $g_\perp \cong 0$. The defect was tentatively identified as interstitial nickel in its singly positive $3d^9$ charge state (Ni_i^+) with a nearby disturbance (perhaps a vacancy or impurity atom) responsible for the trigonal symmetry.

Other studies[2–6] have identified two Ni-related optical transitions with zero-phonon lines at 1.401 and 1.404 eV. Observed in both photoluminescence (PL) and absorption, the transitions were identified as arising between a ground orbital doublet, split by 2.8 meV, and an excited orbital singlet of a single defect. Isotope splittings on the sharp zero-phonon lines, with intensity ratios that matched the abundance ratios of the naturally occurring Ni isotopes, conclusively identified a single Ni atom as part of the defect.[5,6] Uniaxial stress and Zeeman PL studies by Nazaré *et al.*[6] have led to the conclusion that (i) the defect has trigonal symmetry, (ii) both the ground doublet and excited singlet states have effective spins, $S=1/2$, and (iii) the ground-state levels associated with the 1.401- and 1.404-eV transitions have Γ_4 and $\Gamma_{5,6}$ symmetry (of the C_{3v} double group), respectively, while the upper state common to both transitions is Γ_4. In these studies, the g values of the lower state of the doublet, determined from the Zeeman results, agreed approximately with the g values of the EPR study.[1] Both groups of workers[1,6] speculated therefore that the 1.4-eV optical transitions might be associated with the NIRIM-2 defect.

More recently theoretical studies by Paslovsky and Lowther,[7,8] using cluster calculations, showed that it was possible to account for the 1.4-eV transitions as intra-d-shell transitions for interstitial d^9 Ni^+ (although an inconsistency appears between the authors' two publications as to whether the lowest ground state is Γ_4 or $\Gamma_{5,6}$). Such a model had already been shown by Isoya *et al.*[1] to account for the ground-state EPR properties of NIRIM-2. One surprising result remains, however. This is the conclusion of Nazaré *et al.*,[6] that the Zeeman results imply $g_\parallel \sim 0$ and $g_\perp = 2.5$ for the excited state of the optical transition. If true, that is a most unexpected result for an orbital singlet state, and this result has not been addressed in the theoretical studies.

In the present paper we investigate the magnetic circular dichroism in the optical absorption (MCDA) associated with the 1.404-eV Zeeman-split sharp zero-phonon line (ZPL). An attempt to optically detect EPR in the MCDA (MCDA-ODEPR), which would have supplied a critical test of its assignment to the NIRIM-2 EPR center, was unsuccessful. However, from the sign of the MCDA, and the g value of the excited state, we verify unambiguously that the ground-state doublet is $\Gamma_{5,6}$, as concluded by Nazaré *et al.*[6] In addition, we demonstrate in an independent way that, for the excited orbital singlet state, $g_\parallel$ is indeed very close to zero, setting an even lower upper bound. Finally, we develop the interstitial d^9 model further to explore the origin of this unexpected result.

II. SAMPLES

This study was performed using a single-crystal diamond sample on loan to Lehigh from M.H. Nazaré at the University of Aveiro, Portugal. The same sample was also used in previous PL-ODMR studies at Lehigh for which resonances associated with single-substitutional N^0 and substitutional Ni^- were observed.[9] The sample was grown by Kanda using a high-temperature, high-pressure method at the National Institute for Research in Inorganic Materials, in Japan. The sample had been polished into a cuboid with [011], [$0\bar{1}1$], and [100] axes. Ni is introduced as a solvent catalyst in the high-temperature, high-pressure growth process of diamond. The concentration of the Ni-related defect associated with the 1.4-eV band has been estimated[9] from the strength of the absorption band to be 6×10^{12} cm^{-3}, but the overall concentration of Ni is unknown. The concentration of single substitutional N was estimated to be on the order of 10^{19} cm^{-3}.

III. EXPERIMENTAL DETAILS

Experimental setup

The experiments described here were all performed using a tunable titanium:sapphire laser (Coherent model 890). The

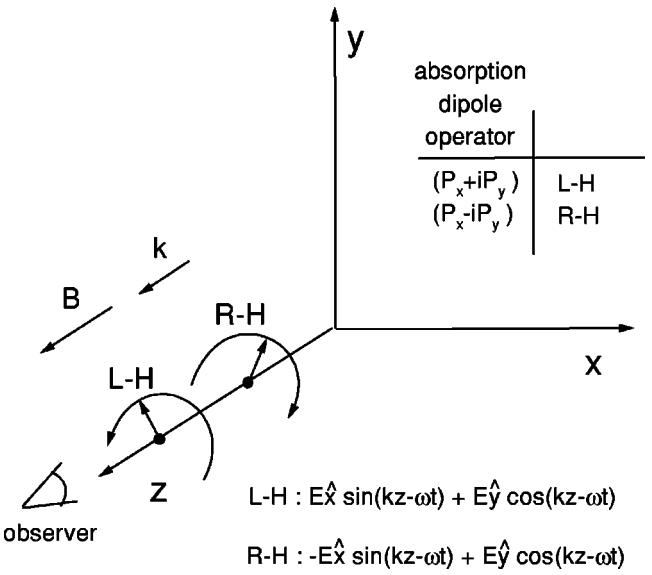

FIG. 1. Definition, in the laboratory system, of the circularly polarized components of light and the corresponding electric-dipole operator to which each couples in an absorption transition.

maximum linewidth specified by the manufacturer was 30 GHz (120 μeV). The incident light was first passed through a linear polarizer (Polaroid, type HN22) and then through a photoelastic quarter-wave modulator (PEM) (Hinds Instruments model No. PEM-90), whose optical axes were placed at a 45° angle to the axis of the polarizer, thereby creating circularly polarized light. The PEM alternated the circular polarization of the light between left- and right-hand polarization at a frequency of 50.2 kHz. This frequency was used as a reference for a lock-in amplifier which measured changes in the transmitted light intensity coherent with the modulation frequency. The transmitted light was detected using a cooled Ge detector (North Coast, model No. EO-817P).

The sample was immersed in liquid He in an Oxford Instruments SM-4 optical cryostat with a built-in superconducting magnet and quartz windows. The sample was mounted, without an aperture-defining mask, in a 35-GHz microwave cavity designed in the form of concentric rings for optical access, allowing for both the MCDA and MCDA-ODEPR studies. For the MCDA-ODEPR studies, 70 mW of unmodulated 35-GHz microwave power from a Gunn oscillator was applied to the cavity, and changes in the MCDA were monitored. To ensure that only light transmitted through the sample was detected, a mask, smaller than the sample image, was placed in front of the detector.

The MCDA for an optical transition of a defect can be defined as[10]

$$X_{\mathrm{MCDA}}=(\alpha_R-\alpha_L)d, \tag{1}$$

where α_L and α_R are the absorption coefficients for left- and right-circularly polarized components of light propagating parallel to the direction of an applied magnetic field, and d is the thickness of the sample. The definitions of the circular components are given in Fig. 1. The right- and left-hand circularly polarized transmitted intensities, I_R and I_L, measured by the detector depend upon the incident intensities produced by the PEM, I_R^0 and I_L^0, according to

$$I_{R,L}=I_{R,L}^0 e^{-\alpha_{R,L}d}. \tag{2}$$

If we have $\alpha_L d,\ \alpha_R d \ll 1$, and $I_R^0=I_L^0$, the relationship between the defect's MCDA and the intensities of transmitted light propagating parallel to the magnetic field can be approximated by

$$X_{\mathrm{MCDA}}=\frac{2(I_L-I_R)}{(I_L+I_R)}. \tag{3}$$

[In the actual experimental setup used, the magnetic-field direction was antiparallel to the light propagation vector **k**. In this case everything is the same, except that the circulation of the electric-field vectors of the left- and right-hand components of the light with respect to the magnetic field is reversed from those appropriate to Eqs. (1) and (3). To correct for this, the signs of the measured MCDA signals were reversed to obtain MCDA values consistent with the definition given in Eq. (1), for $\mathbf{k}\|\mathbf{B}$. [In what follows, therefore, all of the MCDA results, the theoretical treatment, and the discussion, will refer to the conventional setup with $\mathbf{k}\|\mathbf{B}$.]

The phase relationship between the oscillating circularly polarized light produced by the PEM and its reference output used for the lock-in reference signal was determined by removing the sample and inserting between the detector and PEM an analyzer that passed only right-hand or left-hand circularly polarized light. With the proper phase adjustment the lock-in detector was then made to measure directly $I_L - I_R$. In addition to monitoring the difference between I_L and I_R via the lock-in amplifier, the absolute intensity of the transmitted light, $(I_L+I_R)/2$, was also recorded for use in calculating the MCDA signal according to Eq. (3).

IV. EXPERIMENTAL RESULTS

A. Absorption

All of the measurements in the following study were performed at temperatures of either 4.2 or 1.7 K, and thus only transitions involving the lower-lying state of the orbital doublet near 1.404 eV were observed. Shown in Fig. 2 is a typical uncorrected transmission spectrum at $B=0$, exhibiting these transitions. The absorption lines associated with the two most abundant isotopes, ^{58}Ni (67.76%) and ^{60}Ni (26.26%), are indicated.

The relative absorption of the ^{58}Ni isotope is approximately 25% of the incident intensity, thus satisfying the requirement $\alpha d \ll 1$ leading to Eq. (3). The large amplitude background oscillations are due to interference fringes associated with the cryostat windows. In order to suppress these, a series of transmission spectra was taken at a variety of magnetic fields ranging from 0.0 to 2.25 T and is shown in Fig. 3. The light propagation vector was parallel to the crystal [111] direction. A separately run spectrum at $B=0$ T has been subtracted from all the spectra to remove the background oscillations. The positive signal seen for all $B>0$ spectra therefore represents the absorption that is observed for zero field and is not part of the weaker higher-field negative absorption signals, which arise from the Zeeman-split components.

It should be noted that small shifts of the driver controlling the laser frequency occurred during the experiment.

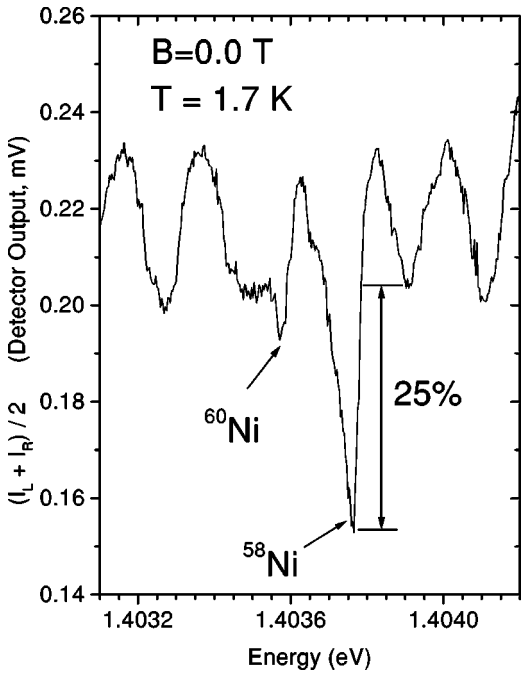

FIG. 2. Transmission spectrum showing the absorption of the two most abundant Ni isotopes. The large background oscillations are interference fringes associated with the cryostat windows.

These shifts were corrected for by comparing the interference fringes on the edges of the uncorrected spectra and then translating them horizontally so they all were aligned with the reference scan. This correction has also been used when necessary for the MCDA spectra of the following sections. Also, the monochromator used to determine the lasing energy was accurate to only about 1.5 meV, the full scan width of the spectra shown. Therefore, for all of the data presented, the zero position of the energy scale has been calibrated by matching the ZPL energy of the ^{58}Ni isotope at $B=0$ T with the corresponding energy previously reported in the absorption spectra.[6]

The two relatively strong positive lines at 1.403 760(5) eV and 1.403 585(5) eV are the zero-field positions of the ^{58}Ni and ^{60}Ni isotopes. The two isotopes are well resolved with a zero-field splitting of 0.175(10) meV, which agrees within experimental accuracy with the value reported by Ref. 6. The full width at half maximum (FWHM) linewidths, $\cong 50(10)$ μeV at T=1.7 K are substantially narrower than those evident in the figures of Ref. 6 ($\cong 100$ μeV). Since the absolute linewidth of the laser is not known (<120 μeV), 50 μeV is an upper limit to the true linewidths of the transitions. Also observed are weaker, negative signals associated with transitions between the individual spin states of the ground and excited states whose degeneracies are removed in the presence of the magnetic field via the Zeeman interaction. These will now be studied more closely via MCDA in the following section.

B. MCDA

The corrected Zeeman MCDA spectra of Fig. 4 were measured for the magnetic field along the crystal [111] direction. A $B=0$ background subtraction technique has been used to remove interference oscillations, similar to that used

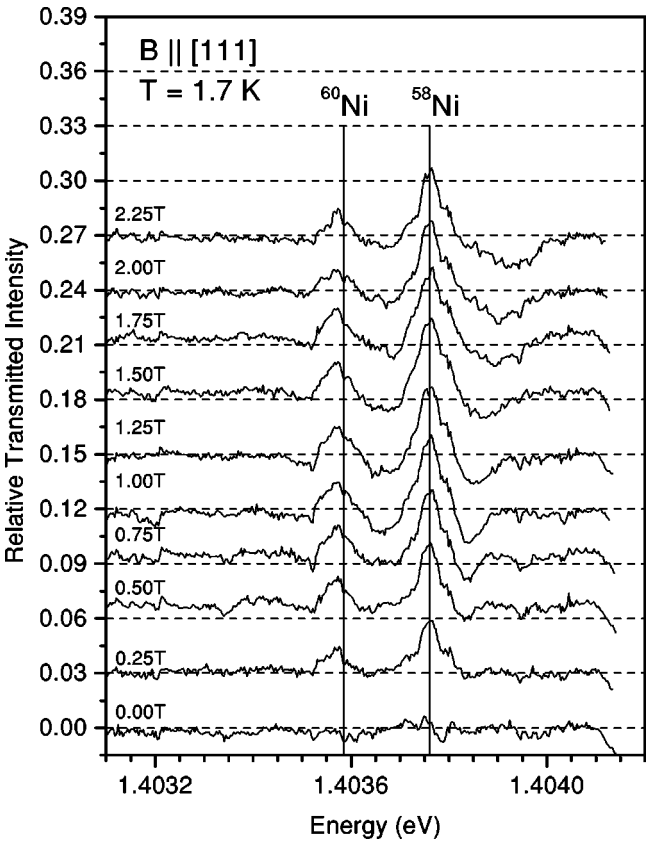

FIG. 3. Transmission spectra at selected magnetic fields for **B**$\|$[**111**] after subtraction of the $B=0$ spectrum to remove the interference fringes. The spectra have been shifted vertically for clarity.

for the absorption spectra of Fig. 3. The absorption signals are strongly left-hand or right-hand circularly polarized, causing the large MCDA signals. Shown in Figs. 5 and 6 are Zeeman MCDA spectra for the magnetic field along crystal [100] and [011] directions, respectively. The background interference fringes were relatively small in Fig. 5 and a reference subtraction was not necessary. It was performed, however, for the data of Fig. 6 .

An intriguing observation can be made for **B** $\|$[011] at $B=0.0$ T. Weak, but nonzero, MCDA signals are observed for the ^{58}Ni and ^{60}Ni isotopes whose spectral shapes and positions are identical to the overall absorption lines, indicating there is an apparent residual MCDA at zero field, an unexpected result. Also the signs of these nonzero signals at 1.7 K were found to be opposite those at 4.2 K. The presence of a small, residual magnetic field does not give an adequate explanation for this finding, and currently it is not understood. This ''zero-field'' MCDA signal was removed from the $B=0.0$ T reference scan prior to being used for background subtraction in Fig. 6.

The data shown in Figs. 2–6 were measured at 1.7 K, the lowest spin state of the ground manifold being predominantly occupied at the higher magnetic fields. In order to observe also the MCDA signals from the higher spin state, a study at 4.2 K of the [100] and [011] data was also performed. Shown in Fig. 7 are the spectra at $B=2.25$ T taken at the two temperatures.

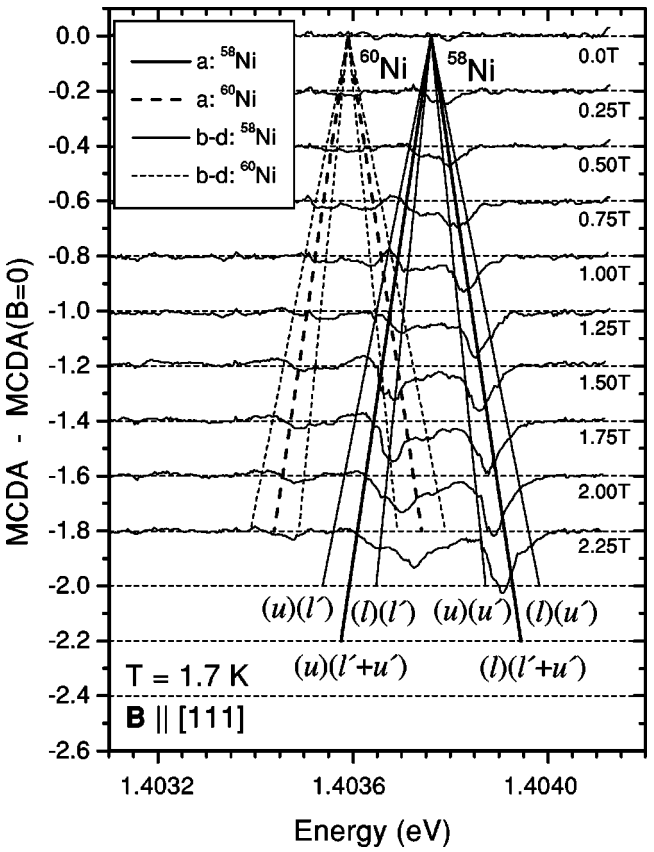

FIG. 4. MCDA spectra for $\mathbf{B}\|[\mathbf{111}]$ compared with the MCDA line positions calculated using the best-fit g tensors given in Table I. The $B=0$ MCDA spectrum has been subtracted from each to remove interference fringes. The labelings of the ^{58}Ni isotope lines represent the lower- (l) and upper- (u) energy Zeeman-split levels of the ground (unprimed) and excited (primed) states in the optical transitions.

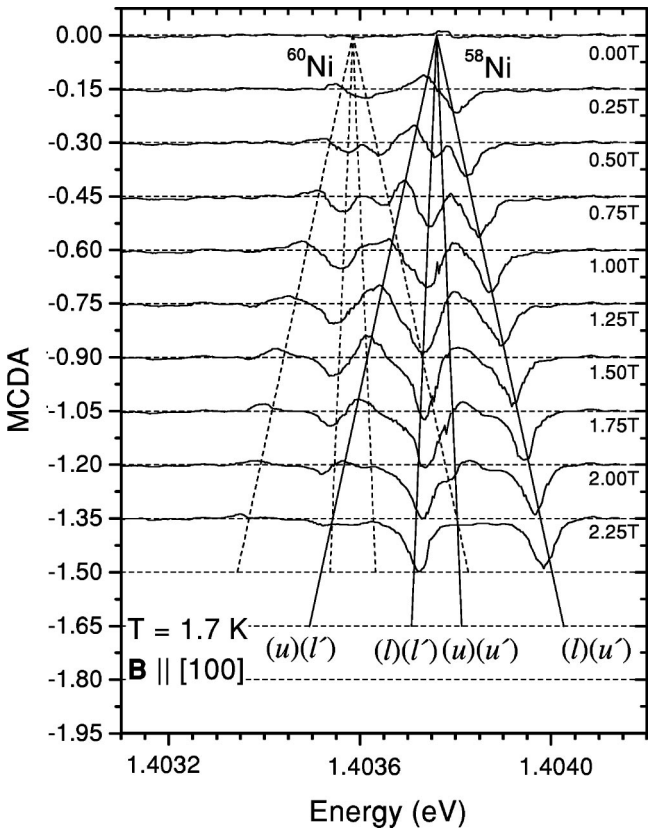

FIG. 5. MCDA spectra for $\mathbf{B}\|[\mathbf{100}]$ compared with best-fit lines calculated using the g tensors of Table I. The labelings follow the convention described in Fig. 4.

1. MCDA-ODMR

The equilibrium population of the Zeeman-split spin states in the ground manifold is given by a Boltzmann distribution between them. Inducing microwave transitions between two spin states, at a rate comparable to the spin-lattice relaxation rate between them, will cause their population difference to decrease, and a change in the MCDA intensity of the optical transition from each will occur. The change will be either an increase or a decrease of the MCDA intensity, depending on whether the optical transition is from the upper- or lower-energy ground spin state, respectively. Attempts to measure such MCDA-ODMR signals by holding the laser frequency fixed and scanning the magnetic field were made. The measurements were difficult because the extremely narrow absorption lines moved as the magnetic field was changed. Measurement schemes, such as magnetic-field sweeps for a series of laser frequency steps, were devised to help alleviate this problem. No MCDA-ODMR signals were observed, but they might have been missed. In addition, however, an EPR transition for a defect with $g_{\perp}=0$ is strictly forbidden for arbitrary orientation of **B** (for our experimental setup where the microwave field is perpendicular to **B**), so it may have been difficult to saturate the transition, made weakly allowed only by strains in the crystal.

2. Spin Hamiltonian fit of the [100] data

What follows is a fit of the Zeeman data of Fig. 5. For a defect of trigonal symmetry (as has been determined by the previous PL stress work[6]) there are four distinct orientations with primary axes along crystal $\langle 111\rangle$ directions. These four axes are labeled a–d in Fig. 8. For the magnetic field applied along the crystal [100] direction the Zeeman spectra of the four orientations will superpose since they share the same angle, 54.7°, with the magnetic field. This simplifies the identification of the lines with the transitions between the individual spin states. The assignment of an effective spin, $\mathcal{S}=1/2$, for both the excited and ground states produces four optical transitions for each isotope. The spectrum taken at 2.25 T shows two dominant negative signals of approximately equal intensity. At this field the populations of the ground-state spin levels have a Boltzmann population ratio of $\cong 6{:}1$, assuming a value of $g\sim 2$. In addition, the ^{58}Ni isotope has a larger intensity by a factor of 2.6 over the ^{60}Ni isotope. Therefore the two large signals can be safely assigned to the transitions between the lower spin ground state and the two excited spin states of the ^{58}Ni isotope.

The reduction in intensity of these two signals at higher temperatures, s_1 and s_3 shown in Fig. 7(a), gives further evidence that this is the correct assignment. The lines s_2, s_4, and s_5 correspondingly grow in intensity, indicating they arise from the upper ground spin state (s_2 and s_4 for the ^{58}Ni isotope; s_5 for the ^{60}Ni isotope). Thus the equal s_1-s_3 and s_2-s_4 energy splittings give the Zeeman splittings of the excited state, the equal s_1-s_2 and s_3-s_4 splittings give the corre-

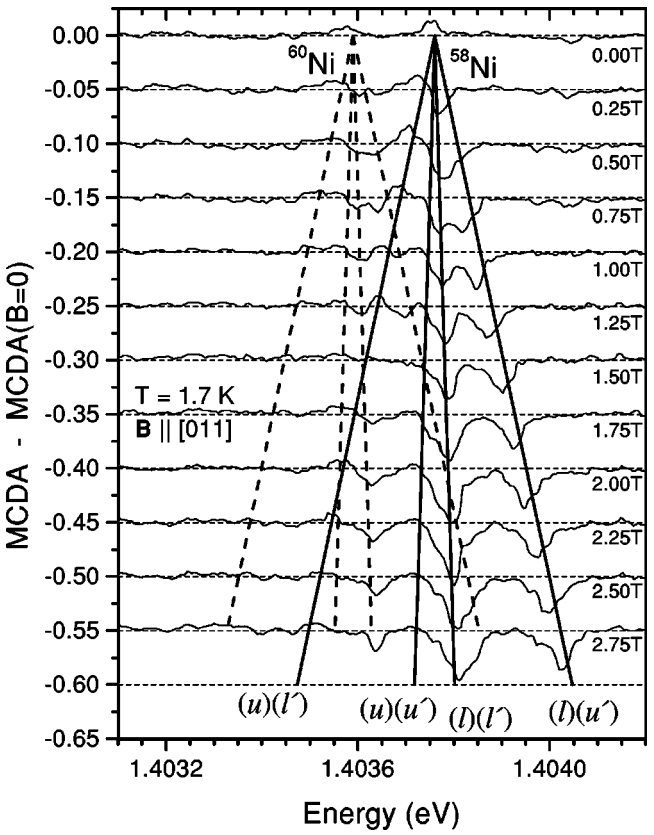

FIG. 6. MCDA spectra for $\mathbf{B}\|[\mathbf{011}]$ compared with best-fit lines calculated using the g tensors of Table I. The MCDA spectrum for $B=0$ has been subtracted from each to remove the interference fringes. The labeling convention follows that described in Fig. 4.

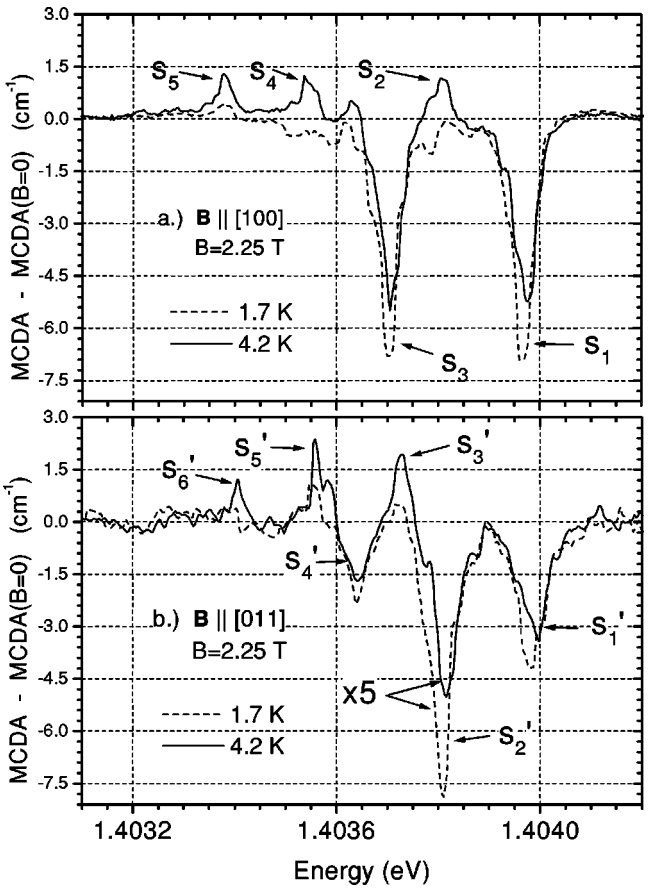

FIG. 7. MCDA spectra taken at temperatures of 1.7 and 4.2 K for two field orientations with $B=2.25$ T.

sponding ground-state splittings, and the easily extracted s_3-s_5 splitting gives the ground-state splitting plus the zero-field isotope splitting. Using the Zeeman Hamiltonian,

$$\mathcal{H}=\mu_B \mathcal{S}\cdot \mathbf{g}_i \cdot \mathbf{B} \tag{4}$$

for the ground ($i=gr$) and excited ($i=exc$) states, the shift of the four Zeeman lines from their zero-field positions become

$$\Delta E=\frac{1}{2}[\pm g_{gr}\pm g_{exc}]\mu_B B. \tag{5}$$

Here the g value in either case is given by

$$g_i=(g_{i\|}^2 \cos^2\theta+g_{i\perp}^2 \sin^2\theta)^{1/2}, \tag{6}$$

where θ is the angle between $\mathbf{B}$ and the defect's trigonal axis. The measured g values that result for $\mathbf{B}\|[100]$ are given in Table I. A fit of the entire data set using these values is included in Fig. 5. The close agreement with the fit confirms the assignments made. All of the MCDA lines are observed throughout most of the magnetic-field range.

The [011] and [111] data are more complicated because, for them, two sets of inequivalent orientations are present, producing a total of eight lines for each isotope in either data set. A model of the defect system will now be discussed to see what insight can be gained before proceeding further.

V. MODEL

Isoya *et al.*[1] suggested that the defect responsible for the NIRIM-2 EPR center was the ground state of interstitial Ni^+ (Ni_i^+) with a nearby vacancy or impurity responsible for the defect's trigonal (C_{3v}) crystal field. Nazaré *et al.*[6] concluded that the optical transitions they observed were between a ground doublet E state (split via spin-orbit interaction) and an excited A_1 state. The following model assigns the optical lines to intra-d-shell transitions of the Ni core, as first proposed by Paslovsky and Lowther.[7] The nature of the ex-

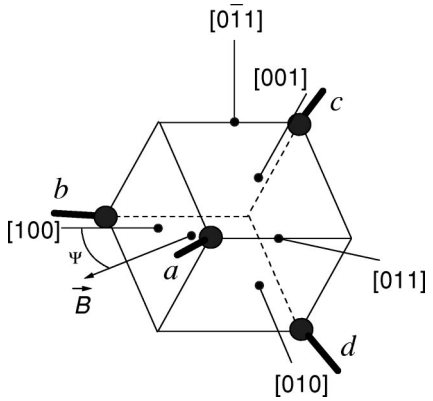

FIG. 8. Illustration showing the four allowed orientations, a–d, of a trigonal (C_{3v}) defect with respect to the cubic axes of diamond. The four trigonal axes are indicated with bold lines.

TABLE I. Effective g values of the ground and excited states measured from the MCDA Zeeman data and our best-fit principal values of the g tensors that result.

	[011] $g_{\text{eff}}(\theta=35.3°)$	[100] $g_{\text{eff}}(\theta=54.7°)$	[111] $g_{\text{eff}}(\theta=0°)$	Best fit $g_{\parallel}$	Best fit $g_{\perp}$
excited	1.38(6)	2.03(6)	$\leqslant 0.10$	0	2.445
ground	2.00(7)	1.23(15)	2.22(20)	2.32	0

pected transitions, including the selection rules, will be explored in detail.

A. Level scheme

Ni_i^+ in Si, according to Ludwig and Woodbury,[11] has an electronic d-shell configuration of $3d^9$ (^2D). This ^2D state (a single hole) splits into doubly and triply degenerate E and T_2 orbital states in the presence of the cubic crystal field produced by the covalent charge distribution on the ligand atoms. For Ni_i^+ in Si the E state is lowest in energy; the crystal field can be viewed as arising from an effective positive charge of the four nearest Si neighbors, or negative charges of the six next-nearest neighbors. This model is assumed to be equally valid for Ni_i^+ in diamond.

The level ordering for Ni_i^+ is closely related to that found for neutral substitutional vanadium in SiC, a system which has recently been explored by Kaufmann *et al.*[12] V_s^0, when occupying the hexagonal substitutional site (the α site) in 6H SiC, differs from the Ni_i^+ system in diamond in two respects: (i) V_s^0 has an electronic configuration $3d^1$ (^2D), (and, for that reason, is referred to as V^{4+} by Kaufmann *et al.*), (ii) it experiences a cubic crystal field of opposite sign (as also observed for substitutional impurities in Si). These two differences each cause an inversion of the E and T_2 levels, and thus the ordering of these two levels ends up to be the same for the two systems. In addition, V_s^0 experiences a relatively weak trigonal field due to the lower symmetry of the 6H SiC host lattice. Therefore the Hamiltonian used[12] for V_s^0 in SiC,

$$\mathcal{H}=\mathcal{H}_{T_d}+\mathcal{H}_{C_{3v}}+\mathcal{H}_{S.O.}+\mathcal{H}_Z, \tag{7}$$

also applies for Ni_i^+, where $\mathcal{H}_{T_d}$ contains the cubic crystal-field term, and the other terms arise from the trigonal crystal field, the spin-orbit interaction, and the Zeeman interaction, in the order listed.

Kaufmann *et al.*[12] expressed the Hamiltonian of Eq. (7) in a basis set whose wave functions are direct products of orbital angular-momentum eigenstates appropriate to $L=2$ and spin states of $S=1/2$. A coordinate system was introduced with $\mathbf{x}'$, $\mathbf{y}'$, and $\mathbf{z}'$ axes, oriented with $\mathbf{z}'$ along the trigonal axis of the defect. The interaction within the $^2T_2$ level was then taken to be

$$\mathcal{H}_{el}(^2T_2)=\frac{2}{5}\Delta_c\mathbf{I}-K\left(L_{z'}^2-\frac{1}{3}L(L+1)\right)+\lambda\mathbf{L}\cdot\mathbf{S}+\mu_B(k\mathbf{L}+2\mathbf{S})\cdot\mathbf{B}, \tag{8}$$

while

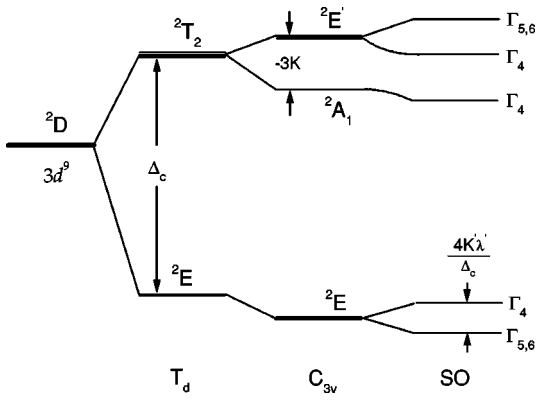

FIG. 9. Energy levels for the ^2D state of interstitial $3d^9$ Ni^+. The effect of the cubic (T_d) and trigonal (C_{3v}) crystal fields and spin-orbit interaction are successively illustrated, as given in the Hamiltonian of Eq. (7).

$$\mathcal{H}_{el}(^2E)=-\frac{3}{5}\Delta_c\mathbf{I}+2\mu_B\mathbf{S}\cdot\mathbf{B} \tag{9}$$

was used for the ^2E level. The parameters Δ_c, K, λ, and k are the cubic crystal-field splitting, one-third of the trigonal crystal-field splitting within the $^2T_2$ state, the spin-orbit parameter, and an orbital reduction factor, respectively. The parameters coupling the $^2T_2$ and ^2E levels were allowed to depart from those used in Eqs. (8) and (9) due to covalency effects. The resulting interaction has the form

$$\mathcal{H}_{el}(^2E,^2T_2)=-K'\left[L_{z'}^2-\frac{1}{3}L(L+1)\right]+\lambda'\mathbf{L}\cdot\mathbf{S}+\mu_Bk'\mathbf{L}\cdot\mathbf{B}, \tag{10}$$

where the corresponding parameters are indicated with primes.

Shown in Fig. 9 are the level orderings, expected in our case for Ni_i^+ in diamond, developed by including successive terms in the Hamiltonian. The irreducible representations used when considering the spin-orbit interaction are those of the C_{3v} double group. The spin-orbit and trigonal field interactions remove the entire orbital degeneracy of the upper T_2 level in first order. The sign of the $^2T_2$ trigonal crystal-field parameter, $K<0$, has been chosen to place the A_1 level lowest in energy. This assignment was made from the PL stress work of Nazaré *et al.*[6] In contrast with the V_s^0 system, the spin-orbit parameters λ and λ' have been taken to be negative, appropriate for a single d^9 hole.

The simultaneous presence of both a spin-orbit interaction and a trigonal crystal field produces a second-order splitting in the ground E state given[12] by

$$E(\Gamma_4)-E(\Gamma_{5,6})=\frac{4\lambda'K'}{\Delta_c}, \tag{11}$$

as shown. The ordering shown in the figure corresponds to the assumption of negative values for both λ' and K'. The principal values of the g tensors associated with the ground-state doublet are, for the $\Gamma_{5,6}$ state,[12,13]

$$g_{\parallel}=2-\frac{4\lambda' k'}{\Delta_c}-\frac{8k'K'}{\Delta_c}, \tag{12}$$

$$g_{\perp}=0,$$

with respect to the $\mathbf{z}'$ axis, and, for the Γ_4 state,

$$g_{\parallel}=2-\frac{4\lambda' k'}{\Delta_c}+\frac{8k'K'}{\Delta_c}, \tag{13}$$

$$g_{\perp}=\frac{4\lambda' k'}{\Delta_c}.$$

The energy of the $\Gamma_{5,6}$ state which derives from the upper T_2 level in Fig. 9 is found from Eq. (8) to be

$$E(\Gamma_{5,6})=-K-\frac{1}{2}\lambda \tag{14}$$

to the accuracy of omitting second-order effects of the coupling (10) to the ^2E ground state, and we have omitted the cubic field energy $2\Delta_c/5$ in writing Eq. (14). To the same accuracy, the energies of the two Γ_4 states from $^2T_2$ are

$$E(\Gamma_4)=\frac{1}{2}K+\frac{1}{4}\lambda\pm\left[\left(\frac{3}{2}K-\frac{\lambda}{4}\right)^2+\frac{1}{2}\lambda^2\right]^{1/2}. \tag{15}$$

Of these states, the one with the lower energy has components

$$|\Gamma_4\alpha\rangle=a|A_1,+\tfrac{1}{2}\rangle-b|T_2^+,-\tfrac{1}{2}\rangle, \tag{16}$$

$$|\Gamma_4\beta\rangle=a|A_1,-\tfrac{1}{2}\rangle+b|T_2^-,+\tfrac{1}{2}\rangle,$$

where

$$a=\cos\gamma, \tag{17}$$

$$b=-\sin\gamma,$$

and

$$\tan 2\gamma=\frac{\lambda/\sqrt{2}}{\frac{3}{2}K-\frac{1}{4}\lambda}. \tag{18}$$

In Eq. (16), the notation $\pm\frac{1}{2}$ designates spin states quantized with respect to the $\mathbf{z}'$ axis, while A_1 denotes the orbital singlet state

$$|A_1\rangle=(|T_2\xi\rangle+|T_2\eta\rangle+|T_2\zeta\rangle)/\sqrt{3}, \tag{19}$$

where $|T_2\xi\rangle$, $|T_2\eta\rangle$, and $|T_2\zeta\rangle$ are the T_2 states transforming like yz, zx, and xy with respect to the cubic axes $\mathbf{x}$, $\mathbf{y}$, $\mathbf{z}$ ($\mathbf{z}'$ is in the [111] direction in this axis system). The other two T_2 states

$$|T_2\theta\rangle=(-|T_2\xi\rangle-|T_2\eta\rangle+2|T_2\zeta\rangle)/\sqrt{6}, \tag{20}$$

$$|T_2\epsilon\rangle=(|T_2\xi\rangle-|T_2\eta\rangle)/\sqrt{2},$$

comprise the orbital E' doublet derived from T_2 in trigonal symmetry (Fig. 9) and transform exactly as do the ground-state doublet components $|E\theta\rangle$ ($\sim 2z^2-x^2-y^2$) and $|E\epsilon\rangle$ [$\sim\sqrt{3}(x^2-y^2)$] under C_{3v} symmetry operations around the $\mathbf{z}'$ ([111]) axis.[14] In Eq. (16), $T_2^{\pm}$ then denotes the states

$$|T_2^{\pm}\rangle=(|T_2\theta\rangle\pm i|T_2\epsilon\rangle)/\sqrt{2}=|E'\pm\rangle. \tag{21}$$

The g factors for the lower Γ_4 state of $^2T_2$, as given by Eq. (16), are then found from the Zeeman term in Eq. (8) to be given by

$$g_{\parallel}=2(a^2-b^2)-2kb^2, \tag{22}$$

$$g_{\perp}=2a^2-2\sqrt{2}kab,$$

where we omit corrections from coupling to the ^2E ground state. For the $\Gamma_{5,6}$ state of $^2T_2$, including these second-order corrections as in Eq. (12), we have

$$g_{\parallel}=2(1-k)+\frac{4\lambda' k'}{\Delta_c}+\frac{8k'K'}{\Delta_c}, \tag{23}$$

$$g_{\perp}=0.$$

B. Development of selection rules

1. Character of the transition

The lifetime of the 1.4-eV luminescence has been measured to be 33 ns.[15] This short lifetime and the strong absorption signals indicate that the transitions are electric-dipole allowed. This type of transition cannot occur between the pure states of a d-shell due to the parity selection rule. Therefore there must be mixing between the d states and other states of odd parity. Recognizing that, in the tetrahedral symmetry of the interstitial site, the T_2 level has the same symmetry as orbital p states, we see that the crystal field may mix in some p character by interaction with higher-lying states. Alternatively, odd-parity states might mix in via hybridization with ligand wave functions. Either interaction would make the transition electric-dipole allowed.

2. Selection rules

Selection rules for transitions induced by circularly polarized light between the ^2E and $^2T_2$ states of Fig. 9 are easily obtained. In trigonal symmetry, using a right-handed coordinate system $\mathbf{x}',\mathbf{y}',\mathbf{z}'$ with $\mathbf{z}'$ along the trigonal axis (taking $\mathbf{x}',\mathbf{y}',\mathbf{z}'$ along the $[\bar{1}\bar{1}2]$, $[1\bar{1}0]$, and [111] with respect to the cubic crystal axes cited previously), we have for the nonzero matrix elements of the components $P_{x'}\pm iP_{y'}$ of the electric-dipole operator between orbital states belonging to the E and A_1 irreducible representations of the C_{3v} point group

$$\langle E'\pm|P_{x'}\mp iP_{y'}|E\mp\rangle=c_2, \tag{24}$$

$$\langle A_1|P_{x'}\mp iP_{y'}|E\pm\rangle=c_1.$$

Here, as indicated in Fig. 1, the positive (negative) sign in the dipole operator corresponds to left (right) circular polarization of light propagating along the $\mathbf{z}'$ direction, and $|E+\rangle$ and $|E-\rangle$ denote states defined as in Eq. (21) in terms of the components $|E\theta\rangle$ and $|E\epsilon\rangle$ of any pair of E states. The upper (lower) sign of $\pm$ or $\mp$ must be taken consistently in each matrix element of Eq. (24). All other matrix elements of

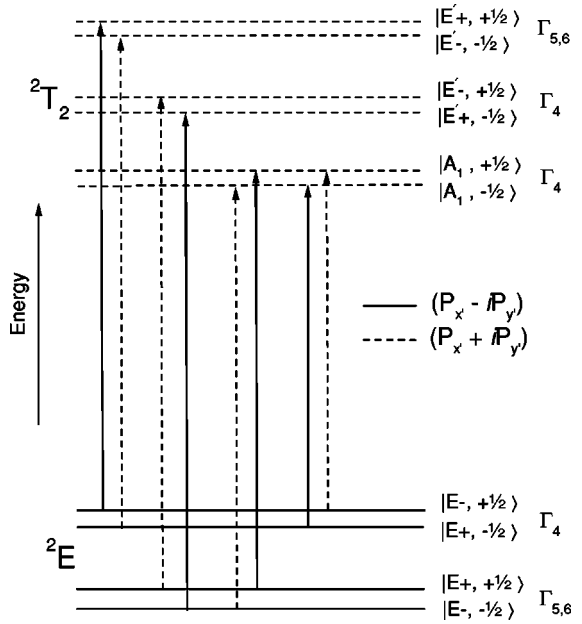

FIG. 10. Diagram of the allowed circularly polarized transitions between ^2E and $^2T_2$ states of the Ni^+ ion in trigonal symmetry obtained from the selection rules for $P_{x'} \pm iP_{y'}$ given in Eq. (24). The + and − designation of individual states denotes the value of the associated spin component $S_{z'} = \pm 1/2$ along the trigonal axis. The splittings and wave functions indicated for the two $\Gamma_{5,6}$ levels and the Γ_4 level derived from the ^2E ground state correspond to their Zeeman split states in a magnetic field of arbitrary direction that has a positive component along $+\hat{z}'$. However, for clarity in illustrating the selection rules, the two excited Γ_4 states are indicated as they would be in the absence of spin-orbit admixing, or of mixing of their $S_{z'} = \pm 1/2$ states due to $g_\perp \neq 0$.

$P_{x'} \pm iP_{y'}$ are zero. [If we approximate the states A_1 and E' as in Eqs. (19) and (20) solely in terms of a triplet state belonging to the representation T_2 of T_d, and if the state E is similarly taken as belonging to the E representation of T_d, then the two parameters $c_1$and c_2 in Eq. (24) may be shown to be equal. The presence of the trigonal field could, however, alter the odd-parity admixtures to the states, causing c_1 and c_2 to differ.]

The ^2E ground state of Ni^+ in tetrahedral symmetry splits in a trigonal field into two Kramers doublets, Γ_4 and $\Gamma_{5,6}$, as given in Eq. (11), when spin-orbit and trigonal-field coupling to $^2T_2$ is included. If we ignore the corresponding small correction to the wave functions, these two doublets comprise the states $|E+,-1/2\rangle$, $|E-,+1/2\rangle$ (Γ_4) and $|E+,+1/2\rangle$, $|E-,-1/2\rangle$ ($\Gamma_{5,6}$), which from Eq. (24) yields the selection rules for $P_{x'} \pm P_{y'}$, given in Fig. 10. Because $g_\perp$ for these two doublets is either exactly zero ($\Gamma_{5,6}$), or very small (Γ_4) according to Eqs. (12) and (13), their first-order Zeeman splittings are due only to the component of a magnetic field along the trigonal axis. With this component taken to be positive ($\mathbf{B}\cdot\mathbf{z}'>0$), the lowest-energy component of each doublet has $S_{z'} = -1/2$, independent of the orientation of **B**, as indicated in Fig. 10. In drawing Fig. 10 to exhibit the selection rules, we have ignored for clarity the spin-orbit mixing of the two excited Γ_4 levels from the $^2A_1$ and $^2E'$ components of $^2T_2$, as given in Eqs. (16)–(18), and also the admixtures of their $S_{z'} = \pm 1/2$ states when **B** is not aligned along the trigonal axis. These will be included in the analysis of the MCDA data in Sec. V B.

3. Off-axis absorption

The selection rules given in Fig. 10 correspond to transitions involving circular components of light whose propagation vector **k** is along the trigonal axis of the defect. However, **k**, defined parallel to $\hat{\mathbf{z}}$ and **B** in the laboratory system, is generally at some angle θ to the defect's trigonal axis $\mathbf{z}'$, the sense of which is to be chosen so that $\mathbf{z}'$ has a positive component along **B** and therefore has θ in the range $0 \leqslant \theta \leqslant \pi/2$. The operators $P_x \pm iP_y$ in the laboratory $\mathbf{x},\mathbf{y},\mathbf{z}$ axis system may be expressed in the defect's axis system as

$$P_x \pm iP_y = \left(\frac{\cos\theta \pm 1}{2}(P_{x'} + iP_{y'}) + \frac{\cos\theta \mp 1}{2}(P_{x'} - iP_{y'}) + P_{z'}\sin\theta \right) e^{\pm i\rho}, \tag{25}$$

where ρ is a phase factor determined by the orientation chosen for **x** and **y** with respect to the $\mathbf{x}',\mathbf{y}',\mathbf{z}'$ axes. The MCDA signal measured for a transition from the initial state, Ψ_i, to the final state, Ψ_f, in the laboratory system ($\mathbf{k}\|\mathbf{B}$) is given from Eq. (1) by

$$(\alpha_R - \alpha_L)d = D(|\langle\Psi_f|P_x - iP_y|\Psi_i\rangle|^2 - |\langle\Psi_f|P_x + iP_y|\Psi_i\rangle|^2), \tag{26}$$

where D is a positive constant. Using Eq. (25), we can reduce Eq. (26) to

$$(\alpha_R - \alpha_L)d = D\cos\theta(|\langle\Psi_f|P_{x'} - iP_{y'}|\Psi_i\rangle|^2 - |\langle\Psi_f|P_{x'} + iP_{y'}|\Psi_i\rangle|^2). \tag{27}$$

[Equation (27) omits a possible contribution to the MCDA from the $P_{z'}\sin\theta$ term in Eq. (25). Since $P_{z'}$ transforms as A_1 under C_{3v}, this term does not contribute for transitions between $\Gamma_{5,6}$ and Γ_4 states, the case that we will conclude is relevant for the 1.404-eV transition of interest in this work.] With off-axis absorption, the MCDA is therefore reduced in magnitude by the factor $\cos\theta$ but retains the same sign as found with **B** along the trigonal axis (since we have $0 \leqslant \theta \leqslant \pi/2$).

The total absorption for the corresponding transition is given by

$$\frac{\alpha_R + \alpha_L}{2}d = \frac{D}{2}(|\langle\Psi_f|P_x - iP_y|\Psi_i\rangle|^2 + |\langle\Psi_f|P_x + iP_y|\Psi_i\rangle|^2), \tag{28}$$

which, to the same approximation (ignoring the $P_{z'}$ term), with Eq. (25), becomes

$$\frac{\alpha_R + \alpha_L}{2}d = \frac{D}{4}\{(\cos^2\theta + 1)(|\langle\Psi_f|P_{x'} - iP_{y'}|\Psi_i\rangle|^2 + |\langle\Psi_f|P_{x'} + iP_{y'}|\Psi_i\rangle|^2) + (\cos^2\theta - 1)(\langle\Psi_f|P_{x'} - iP_{y'}|\Psi_i\rangle \times \langle\Psi_f|P_{x'} + iP_{y'}|\Psi_i\rangle^* + \text{c.c.})\}, \tag{29}$$

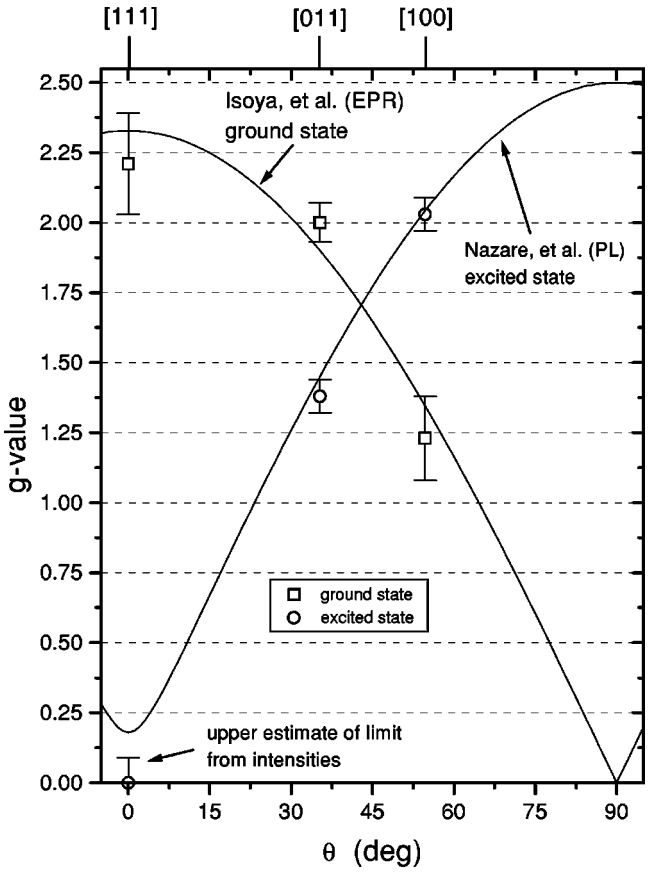

FIG. 11. Measured g values at the three orientations relative to the defect trigonal axis that were studied. The solid lines represent the g tensors determined previously by Nazaré *et al.* (Ref. 6) and Isoya *et al.* (Ref. 1) for the excited and ground states, respectively.

where the cross term, which vanishes for the MCDA, Eq. (27), must be retained.

VI. COMPARISON WITH EXPERIMENTAL RESULTS

A. g-value determinations

We are now prepared to return to the [011] MCDA results. In that case, the propagation direction **k** is perpendicular to the $\mathbf{z}'$ axes of defects c and d in Fig. 8. For them, $\theta=90°$, and therefore Eq. (27) reveals that they produce zero MCDA. The analysis is therefore simplified in that only the two equivalent a and b orientations give rise to the MCDA signals. Further, at the highest field only their lowest-energy ground spin state will be thermally populated. In analogy to the [100] fit in Sec. IV A 2, the two largest signals of Fig. 6 are therefore assigned to transitions from the lowest ground spin state of the ^{58}Ni isotope. The temperature dependence of Fig. 7(b) shows the intensity of the two peaks to be reduced at higher temperatures, further verifying the assignment. The energy splitting between s_1' and s_2' is assigned to the excited state, while that between s_1' and s_3' belongs to the ground state. Effective g values, using Eq. (5), were calculated and are included along with the [100] data in Table I. Shown in Fig. 11 is a plot of these values versus the dependence predicted with the values reported by Isoya *et al.*[1] and Nazaré *et al.*[6] for the ground and excited states, respectively. Our g values agree with theirs within experimental error.

In particular, the [100] and [011] data agreement with the excited state estimates of Nazaré *et al.* appear generally consistent also with their estimate of $g_\parallel\sim 0$. An independent demonstration that this unexpected result is indeed correct can also be obtained from the relative intensities of the MCDA transitions. As can be seen in Figs. 5 and 7, with $\mathbf{B}\|[100]$, the two transitions from the lower ground spin state have the same sign but additionally have approximately *equal amplitudes.* As we will now show, this requires that $g_\parallel\sim 0$ for the excited state.

Expressing Eq. (4) in the x',y',z' defect axis system, with **B** in the $x'z'$ plane, we have for the effective spin Hamiltonian for the excited state

$$\mathcal{H}=\mu_B B[g_\perp \sin\theta \mathcal{S}_{x'}+g_\parallel \cos\theta \mathcal{S}_{z'}]. \tag{30}$$

The value $g_\perp=2.5$ for the excited state unambiguously rules out its identification as the $\Gamma_{5,6}$ state, for which, according to Eq. (23), and proven more generally in Ref. 12, $g_\perp$ is rigorously zero. The excited state must therefore be a Γ_4 state, consistent with the level ordering given in Fig. 9. As a result, Eq. (30) leads to the eigenstates

$$|\Psi_{f1}\rangle=\sin\delta|\Gamma_4\alpha\rangle+\cos\delta|\Gamma_4\beta\rangle, \tag{31}$$

$$|\Psi_{f2}\rangle=-\cos\delta|\Gamma_4\alpha\rangle+\sin\delta|\Gamma_4\beta\rangle,$$

in terms of the states of Eq. (16), where

$$\cos 2\delta=-\frac{g_\parallel\cos\theta}{\sqrt{g_\perp^2\sin^2\theta+g_\parallel^2\cos^2\theta}}. \tag{32}$$

To relate $\cos 2\delta$ to the MCDA, we evaluate the latter from Eq. (27) for the transitions from the lowest Zeeman level of the ground state to the two states, Ψ_{f1} and Ψ_{f2}, of Eq. (31), using Eqs. (16) and (24), giving if the ground state is $\Gamma_{5,6}$,

$$(\alpha_R-\alpha_L)d=-\frac{D}{2}\cos\theta\{a^2c_1^2-b^2c_2^2\pm(a^2c_1^2+b^2c_2^2)\cos 2\delta\}, \tag{33}$$

or, if the ground state is Γ_4,

$$(\alpha_R-\alpha_L)d=+\frac{D}{2}a^2c_1^2(1\pm\cos 2\delta). \tag{34}$$

In each, the + sign goes with the transition to Ψ_{f1}, the − sign with that to Ψ_{f2}. For either of these two possibilities, equal intensities for the two transitions requires $\cos 2\delta=0$, corresponding to equal admixtures of $|\Gamma_4\alpha\rangle$ and $|\Gamma_4\beta\rangle$ in each Zeeman-split level, and from Eq. (32), this requires $g_\parallel=0$. (In the next section, it will be possible to establish an upper limit $g_\parallel\leqslant 0.10$.)

Therefore, having confirmed in this way that, for the excited state, $g_\parallel\sim 0$, the largest intensity single peak for the [111] data of Fig. 4 can now be identified as belonging to the superposed $|l\rangle|l'\rangle$, $|l\rangle|u'\rangle$ transitions for the defect orientation aligned along **B**, the splitting of the upper state being negligible. The shift from the zero-field position therefore provides a direct measure of the ground state value of $g_\parallel$,

which is also included in Table I and Fig. 11. The best fit to our experimental data points yields excited and ground state g tensors that are also included in Table I. The resulting Zeeman dependencies compared to the [011], [100], and [111] MCDA data are shown in Figs. 4, 5, and 6.

B. Identification of the transitions

As established in the previous section, the values $g_\perp = 2.5$, $g_\parallel \approx 0$ for the excited state identify it as a Γ_4 state, consistent with the level ordering given in Fig. 9. From Eq. (22), we find that these g values can indeed arise for the lower Γ_4 state if $k = 0.89$, giving for the admixture coefficients $a = 0.81$, $b = -0.59$. From Eqs. (17) and (18), these coefficients in turn give $\lambda = 3.1K$.

The sign of the experimentally observed MCDA transitions is negative. Therefore, the ground state cannot be Γ_4, because the MCDA predicted for it is always positive, as given by Eq. (34). The ground state is therefore unambiguously identified to be $\Gamma_{5,6}$, as indicated in Fig. 9, and Eq. (33) is appropriate for the Zeeman-split optical transitions. With $\cos 2\delta = 0$, the result when **B** departs from the defect z' axis, this reduces for the transitions to

$$(\alpha_R - \alpha_L)d = -\frac{D}{2}\cos\theta(c_1^2a^2 - c_2^2b^2). \tag{35}$$

A similar calculation for the total absorption of each transition, using Eqs. (16), (24), and (29) gives

$$\frac{\alpha_R + \alpha_L}{2}d = \frac{D}{2}\left\{\frac{\cos^2\theta + 1}{4}(c_1^2a^2 + c_2^2b^2) \pm \frac{1 - \cos^2\theta}{2}c_1c_2ab\right\}, \tag{36}$$

where the $\pm$ sign depends upon which of the excited-state Zeeman-split states is involved. At $B = 0$, where all four transitions between the Zeeman-split ground and excited states superpose, as do the contributions from the four equivalent defect orientations, the complex angular dependence disappears and Eq. (36) simplifies to

$$\frac{\alpha_R + \alpha_L}{2}d = 4\frac{D}{3}(c_1^2a^2 + c_2^2b^2), \tag{37}$$

where the factor of four includes the contribution of the four differently oriented defects.

From Eq. (35), it is clear that the admixture coefficient b required to obtain $g_\parallel = 0$ introduces a component of the opposite sign to the MCDA, reducing its magnitude. This therefore provides an additional test of the model. In making this test, we experimentally estimate the ratio of the MCDA signal for a particular transition to the unsplit absorption at $B = 0$. We compare this to the ratio of Eq. (35), properly weighted for the Boltzmann occupancy of the ground Zeeman-split state of the transition and the number of equivalent orientations, to Eq. (37), and solve for $c_2^2b^2/c_1^2a^2$. For this comparison, we take the experimental results for $B\|[100]$, where all four defect orientations are equivalent, thus avoiding errors due to possible preferential defect alignment. Using the MCDA magnitude of the high-energy split component, which, as can be seen in Fig. 5, is free of overlapping transitions, we obtain for the ratio ~ 0.7, which is reduced only slightly from the unadmixed ($b = 0$) value of $\sqrt{3}/2 = 0.866$. This gives $c_2^2b^2/c_1^2a^2 \sim 0.1$. To be consistent with the values $a = 0.81$, $b = -0.59$ requires $c_2/c_1 \approx 0.45$.

We are now prepared to make an upper limit estimate for $g_\parallel$ in the excited state. If we allow a small ϵ% difference between the intensity of the two MCDA signals, Eq. (33) leads to

$$|\cos 2\delta| \leqslant \left(\frac{\epsilon}{100}\right)\frac{|a^2c_1^2 - b^2c_2^2|}{2(a^2c_1^2 + b^2c_2^2)}. \tag{38}$$

We estimate from the [100] results, Fig. 5, that the intensities of the two well-resolved lines are equal within $\epsilon = 7\%$. With $c_2^2b^2/c_1^2a^2 \sim 0.1$, this gives $|\cos 2\delta| \leqslant 0.03$, which with Eq. (32), gives $g_\parallel \leqslant 0.10$, which is an even lower limit than that given by Nazaré *et al.* ($\leqslant 0.18$). This estimate has been included in Table I and Fig. 11.

VII. DISCUSSION

Our MCDA studies have therefore independently confirmed in detail the conclusions of Nazaré *et al.*[6] that the 1.404-eV transition is from a ground $\Gamma_{5,6}$ state to a Γ_4 excited state in C_{3v} symmetry, and they have also confirmed the g values that were estimated for the two states. Expanding upon a treatment by Paslovsky and Lowther,[7] we have shown further that all of the general experimental features can be explained satisfactorily as arising from internal transitions within the $3d^9$ configuration of the interstitial Ni^+ ion as perturbed by the cubic and trigonal crystal fields and spin-orbit interaction. The level ordering is illustrated in Fig. 9.

We have also shown that the unusual g values for the excited Γ_4 state can be explained by spin-orbit-induced admixtures between it and the other Γ_4 excited state. As opposed to the rigorous $g_\perp = 0$ result for $\Gamma_{5,6}$, the $g_\parallel \approx 0$ result for the Γ_4 state is purely accidental. It results from the fortuitous relative magnitudes for the spin-orbit parameter λ and the trigonal crystal-field parameter K, i.e., $\lambda = 3.14K$. The required admixtures, $a = 0.81$ and $b = -0.59$ in Eq. (16), are, in turn, consistent with the magnitudes of the observed MCDA if the optical matrix elements to the A1 (c_1) and E' (c_2) excited states are different, with $c_2/c_1 \sim 0.45$. Since the existence of finite matrix elements between these states results primarily from small admixtures of odd-parity states outside of the d manifold, this implies that the degree of admixture is significantly affected by the trigonal component of the defect symmetry.

Let us therefore further explore how well the simple crystal-field model works in describing the ^2E ground state. The measured separation between the $\Gamma_{5,6}$ and Γ_4 levels of ^2E, 22.4 cm^{-1}, together with the value for the cubic field splitting $\Delta_C \sim 11\,300$ cm^{-1}, yields from Eq. (11) a value for the product $\lambda' K' \sim +63\,200$ cm^{-2}. Were we to assume $\lambda = \lambda'$, appropriate for a pure crystal-field model without covalency, and $K = K'$, these values for $\lambda' K'$ and λ/K would enable us to evaluate $\lambda = \lambda' = -446$ cm^{-1} and $K = K' = -142$ cm^{-1}. This is certainly a reasonable value for λ, which for the free Ni^+ ion has a value -603 cm^{-1},[16] while

the value for K' represents a weak trigonal field.

There are problems, however, when we attempt in this simple model to interpret the published experimental values $g_{\|}(\Gamma_{5,6})=2.3285$ and $g_{\|}(\Gamma_4)=1.62$ for the two spin-orbit levels of the ^2E ground state.[1,6] From the sum and difference of these values, using Eqs. (12) and (13), we obtain $\lambda' = +73/k'\ \mathrm{cm}^{-1}$ and $K' = -502/k'\ \mathrm{cm}^{-1}$. The positive sign of λ' is clearly unacceptable, being inconsistent with the d^9 character of the Ni^+ ion, the observed level ordering in the ground and excited states, and the positive $\lambda' K'$ product given by Eq. (11). Because the value for $g_{\|}(\Gamma_{5,6})$ is known accurately from EPR measurements, it appears that the difficulty may lie with the value for $g_{\|}(\Gamma_4)$, which was determined from difficult optical Zeeman experiments and for which no estimate of accuracy was given. For example, a value for $g_{\|}(\Gamma_4)=2$ would give $\lambda' = -464/k'\ \mathrm{cm}^{-1}$ and $K' = -232/k'\ \mathrm{cm}^{-1}$, again reasonable values, although their product would then exceed that estimated from Eq. (11) for the level splitting. In fact, it is not possible to *simultaneously* satisfy Eqs. (11)–(13), except in the narrow range $1.67 \leqslant g_{\|}(\Gamma_4) \leqslant 1.79$, which, with $g_{\|}(\Gamma_4)=1.79$, gives $\lambda' = -167/k'\ \mathrm{cm}^{-1}$, $K' = -380/k'\ \mathrm{cm}^{-1}$, and requires $k' = 1$. There is no requirement, of course, that $\lambda=\lambda'$, or $K=K'$, so such a reversal in relative magnitudes from the $\lambda/K=3.14$ result for the excited state is possible. Even in the pure crystal-field model, K and K' depend upon different combinations of the averages $\langle r^2\rangle$ and $\langle r^4\rangle$ of the electron radial distribution on the Ni ion,[17] while λ and λ' can differ if covalency is important. However, in diamond, with its large band gap, and the small spin-orbit parameter of the host carbon atom, such covalency contributions are expected to be small, and such a large reduction in λ' from the free ion value of $-603\ \mathrm{cm}^{-1}$ is unexpected. In fact, covalency effects might normally be expected to make $|\lambda'|>|\lambda|$, as found for the vanadium ion ($3d^1$) in 6H-SiC in the analysis of Kaufmann *et al.*,[12] not the reverse.

Therefore a detailed and fully acceptable quantitative fit, including, in particular, the g values and level splittings, does not appear possible within a simple pure crystal-field model alone. In particular, in our treatment, contributions to the g values and level splittings arising from states outside the $3d^9$ configuration of Ni^+ have not been considered. Also, vibronic effects have not been considered, although we believe them to be small in this case. As noted above, quite small shifts in the experimental g values can significantly alter the values of λ' and K' deduced from Eqs. (12) and (13). Conversely, small additional contributions to these equations would have the same effect, and it is quite possible therefore that such corrections are necessary for a quantitative fit. Indeed Paslovsky and Lowther[7] have proposed that mixing with the $4p$ states of the Ni^+ ion may contribute significantly to the splitting of ^2E, and such corrections have also been proposed by Scherz[18] and Telahun *et al.*[19] in the case of Cu^{2+}, another $3d^9$ ion, in various II-VI hosts.

In order to help sort out these finer details, it would be highly desirable to establish the transition energies to the other two excited states. Unfortunately, however, sharp additional zero-phonon transitions that could be assigned to these transitions have not been reported. With $\lambda \sim -440\ \mathrm{cm}^{-1}$, and $\lambda=3.14K$, Eqs. (14) and (15) predict for the crystal-field model the positions of the upper Γ_4 and $\Gamma_{5,6}$ excited-state levels to be at ~ 760 and $\sim 920\ \mathrm{cm}^{-1}$ above the lower Γ_4 level, respectively. The transitions to these states would therefore fall in the region where strong one-phonon-assisted structures to the main 1.404-eV line exist. The failure to detect them could result from the coupling of these states to the one-phonon excited states of the lower Γ_4 level, which could serve to severely broaden them.

VIII. SUMMARY

The conclusion of Nazaré *et al.*[6] that the 1.404-eV optical transition is from a ground $\Gamma_{5,6}$ state to a Γ_4 excited state of Ni^+ in C_{3v} symmetry has been independently confirmed by our MCDA studies, as have the g values that they deduced for the two states. We have shown that the general features of the optical spectrum are explained satisfactorily as arising from internal transitions within the $3d^9$ configuration of interstitial Ni^+ ion as perturbed by the cubic and trigonal crystal fields and spin-orbit interaction. We have demonstrated in particular that the unusual g values found for the excited Γ_4 state can be understood within the crystal-field model with reasonable values for the crystal-field and spin-orbit parameters. Detailed *quantitative* agreement with the ground-state g values has not been achieved, however. This presumably reflects the need to include other minor contributions such as can arise from including states outside of the $3d^9$ manifold.

Note added in proof. G. Davies (in a private communication) has kindly reanalyzed the results of Ref. 6, and concludes that $g_{\|}(\Gamma_4)\cong 2$ is well within the accuracy of their data. The principal failure of the simple crystal field model may therefore be in accounting for the ^2E splitting, as proposed by Scherz[18] and Telahun.[19]

ACKNOWLEDGMENTS

We gratefully acknowledge the important roles of H. N. Nazaré, who loaned the crystal to us for the study, and of H. Kanda, who initially grew and supplied the crystal to her. This research was supported jointly by the National Science Foundation, Grant No. DMR-97-04386, and the Office of Naval Research, Electronics Division, Grant No. N00014-94-10117.

*Present address: Lucent Technologies, 9333 S. John Young Pkwy., Orlando, FL 32819.

[1] J. Isoya, H. Kanda,. and Y. Uchida, Phys. Rev. B **42**, 9843 (1990).

[2] A. T. Collins and P. M. Spear, J. Phys. C **16**, 963 (1983).

[3] A. T. Collins, J. Phys.: Condens. Matter **1**, 439 (1989).

[4] A. A. Gippius, V. S. Vavilov, A. M. Zaitsev, and B. S. Zhakupbekov, Physica B & C **116B**, 187 (1983).

[5] G. Davies, A. J. Neves, and M. H. Nazaré, Europhys. Lett. **9**, 47 (1989).

[6] M. H. Nazaré, A. J. Neves, and G. Davies, Phys. Rev. B **43**, 14 196 (1991).

[7] L. Paslovsky and J. E. Lowther, J. Phys.: Condens. Matter **4**, 775 (1992).
[8] J. E. Lowther, Phys. Rev. B **51**, 91 (1995).
[9] M. H. Nazaré, P. W. Mason, G. D. Watkins, and H. Kanda, Phys. Rev. B **51**, 16 741 (1995).
[10] J. M. Spaeth, J. R. Niklas, and R. H. Bartram, *Structural Analysis of Point Defects in Solids* (Springer-Verlag, New York, 1992), p. 87.
[11] G. W. Ludwig and H. H. Woodbury, Phys. Rev. Lett. **5**, 98 (1960).
[12] B. Kaufmann, A. Dörnen, and F. S. Ham, Phys. Rev. B **55**, 13 009 (1997).
[13] In Ref. 12, K' was mistakenly substituted for k' in the second term of both Eqs. (8b) and (8c), which should read $-4\lambda' k'/\Delta_C$, in agreement with Eq. (B7) of Ref. 12, and with Eqs. (12) and (13) of this paper.
[14] G. F. Koster, J. O. Dimmock, R. G. Wheeler, and H. Statz, *Properties of the Thirty-Two Point Groups* (MIT Press, Cambridge, 1963), p. 55.
[15] M. Crossfield, Ph.D. thesis, University of London, 1978.
[16] C. E. Moore, *Atomic Energy Levels*, Natl. Bur. Stand. (U.S.) Circ. No. 467 (U.S. GPO, Washington, D.C., 1949).
[17] D. S. McClure, J. Chem. Phys. **36**, 2757 (1962).
[18] U. Scherz, J. Phys. Chem. Solids **30**, 2077 (1969).
[19] T. Telahun, U. Scherz, P. Thurian, R. Heitz, A. Hoffmann, and I. Broser, Phys. Rev. B **53**, 1274 (1996).